UCRL-92441
PREPRINT

INITIAL RESULTS FOR THE FAILURE STRENGTH OF A LOVA GUN PROPELLANT AT HIGH PRESSURES AND VARIOUS STRAIN RATES

Marc Costantion
Donald Ornellas

JANNAF Propulsion Meeting
San Diego, CA
April 9-12, 1985

April 1985

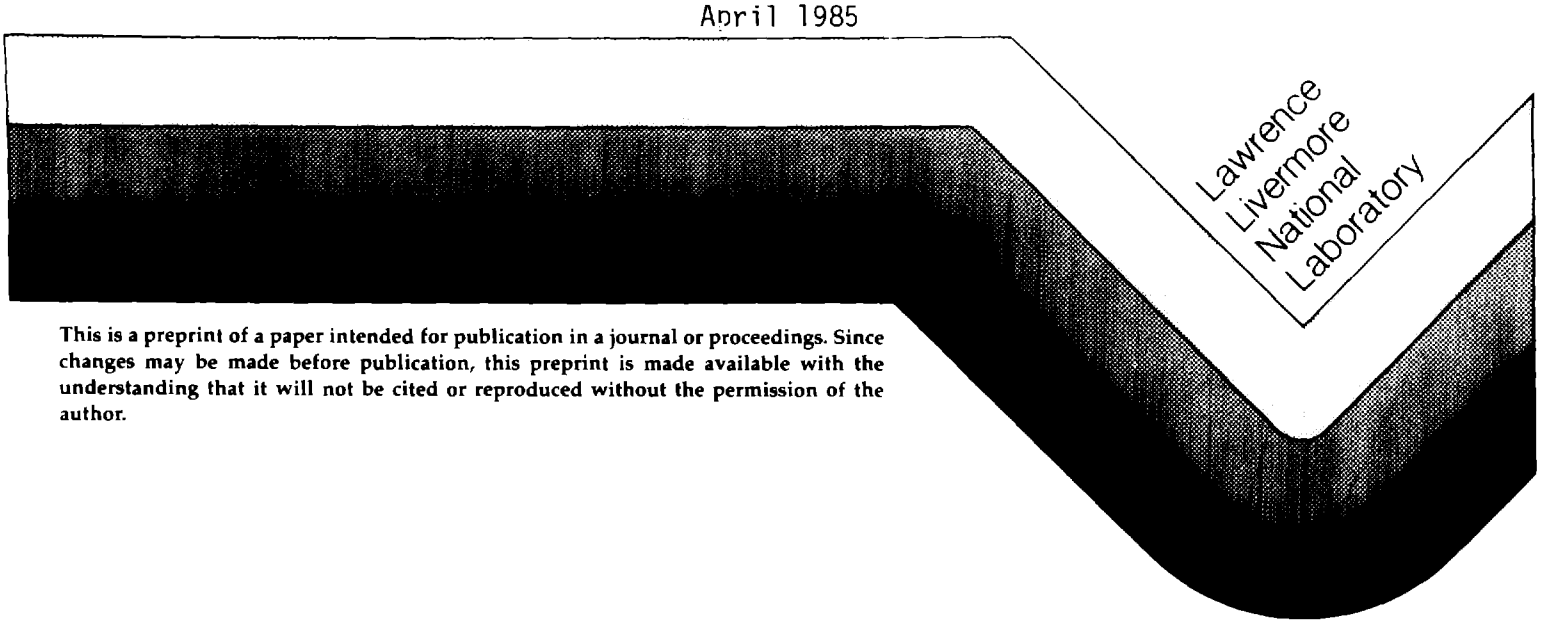

ABSTRACT

We present the initial results for the failure strength of a LOVA gun propellant at high pressures and various strain rates. We believe these to be the first such data for these conditions. Right circular cylinder samples are loaded hydrostatically to pressures of up to 400 MPa (60,000 Psi) then, holding this confining pressure constant, an additional axial load is applied to create a shear stress. Shear stress as a function of axial strain is measured and values at 3% and 5% axial strain are reported at strain rates of 10^{-4}, 10^{-2}, 10^{-1}, and 10^{3} s^{-1} at various confining pressures to 400 MPa. The strength at 10^{-4} s^{-1} increases by more than a factor of six over 400 MPa with an increasing slope. Similar rates of increase are found for strain rates of 10^{-2} and 10^{-1} s^{-1}. We are unaware of this type of behavior in any other material. At 0.1 MPa confining pressure, the strength increases by almost a factor of 5 as the strain rate increases from 10^{-4} to $2.6(10^{3})$ s^{-1}. The implications of these data to gun propellant grain design and the vulnerability of LOVA propellants are discussed.

INTRODUCTION

The high pressure mechanical equation of state of the propellant grains making up a gun charge play a fundamental role in both normal and abnormal interior ballistic cycles. Most attempts to understand the propagation of the burn front, both to optimize grain performance and to avoid the deflagration to detonation transition, involve as a first order effect the mechanical response of the propellant grain. This response is important in two ways. Theoretical models usually involve a two phase hydrodynamic flow in which the constitutive relations for both the porous material (packed bed) and the solid phase (which itself may be porous) are required in the conservation equations for momentum and energy[1]. These treatments, while relatively sophisticated, still use only a hydrostatic stress [$\sigma_{ij} = P$, $(i = j)$; $\sigma_{ij} = 0$ $(i \neq j)$]. Constants, such as the bulk and shear moduli and Poisson's ratio, in the mechanical equation of state are not known from experiments and either are estimated or used as fitting parameters. The intuitively important physics of shear stresses that cause particle deformation and fracture have been included only recently[2], using ideas from porous materials[3] and soil mechanics[4]. There are few data[5,6] for energetic materials specifying these empirical relationships between stress and the response of a packed bed or porous grain.

While this response is important in optimizing grain design and propellant porosity, it is critical in understanding an abnormal interior ballistic cycle, in which a transition occurs from a normal burning rate to detonation. One quite possible mechanism for this transition is the creation of an abnormally high total surface area of the burning propellant because of deformation and fracture of propellant grains[7]. In this case, the grains making up the loosely packed bed of a gun charge are accelerated by hot gases and collide with each other, the breech walls, and the base of the projectile. These impacts produce large shear stresses at high strain rates which, under certain conditions, result in failure of the grain. The burning fragments, having a greater total surface area than the original grain, increase the rate of gas evolution so that the relative quickness (dP/dt) of the burn exceeds the normal range[7].

Figure 1 shows a typical failure curve through a slice of maximum shear stress-confining pressure ($\tau_m - \sigma_3$) space. A solid can support stress states that fall between the curve and the σ_3 axis, while states above the curve result in brittle or ductile failure. Both the curve itself and the transition between brittle and ductile failure are functions of the strain rate and the temperature. Modern approaches to describing the response of the material to stress use finite element or finite difference techniques, in which the strain in an element is used to calculate the stress for the next time step. Should this stress fall within the failure envelope, the solid is still competent and normal burning continues. However, if the new stress state lies outside the envelope, it is relaxed back to the curve (or to a residual strength curve), and the material flows or fragments. In the former case a "plug" forms and calculations show a transition to detonation[8]. In the latter case, the total surface area and the derivative dP/dt increase.

Data for the mechanical equation of state at high pressures and strain rates matching the conditions of the ballistic cycle are rare. While there are some results for rocket propellants at high strain rates and moderate pressures[9], for gun propellants at room pressures and high strain rates[10-12] and at high pressures and low strain rates[13]; we believe these to be the first data for high pressures and high strain rates. These are the initial results in a program to define the failure strengths of three main tank gun propellants, LOVA, M30A1, and JA2, over the pressure range 0.1-400.0 MPa (15-60,000 Psi) and strain rates of 10^{-4} to 10^{3} s^{-1} at room temperature. The ranges covered by these initial results are: 1) at 10^{-4} s^{-1}, $0.1 < P < 400$ MPa; 2) at 10^{-2} s^{-1}, $0.1 < P < 200.0$ MPa; 3) at 10^{-1} s^{-1}, $0.1 < P < 30.0$ MPa; and 4) at 10^{3} s^{-1}. P = 0.1 MPa.

SAMPLES

The composition of this LOVA is given in Table 1. The samples were received from Dr. Robert Lieb of the Ballistic Research Laboratory in June 1984 in taped-shut, plastic boxes and stored in an LLNL magazine under ambient conditions of temperature and pressure until use. The samples were right cylinders 2.54cm long and 1.19cm in diameter (except for the Hopkinson split bar samples). The cross-section of the cylinder was elliptical, evidently owing to relaxation during drying after the propellant was extruded. There was a nominal difference of about 0.15mm between the major and minor axes of the cross section, with an average diameter of about 1.19cm. The ends were prepared by dry-polishing with 280 then 600 grit silicon carbide paper so that they were smooth and parallel to .025mm.

Test samples were prepared by shrinking onto a mandrel a length of polyolefin (heat shrinkable) tubing, then gently pushing into the tubing the sample and endpieces. The polyolefin jacket was secured to each endpiece using two pieces of wire. This method, perfected by Howard Washington of LLNL, rarely fails to prevent leakage of high pressure oil into the sample. For the samples used at intermediate strain rates, where the pressure fluid is argon or nitrogen, a silicone rubber adhesive is added at the jacket-endpiece interface.

EXPERIMENTAL

The general approach to this type of experiment is to subject a right circular cylinder sample to a hydrostatic confining pressure and then to apply an additional load along the axial direction, keeping the confining pressure constant (Fig 1). The measured quantities are the confining pressure, the axial load, and the axial displacement; resulting in curves similar to the one shown in Fig. 2. The calculated quantities are the maximum shear stress (throughout this paper the "shear stress") ($\tau_{max} = (\sigma_1 - \sigma_3)/2$), the

axial strain ($\varepsilon_1 = \Delta L/L_0$), and an estimate of the effective Young's modulus. The shape of the curve also indicates the type of failure. If the material fails brittlely, the maximum shear stress drops suddenly at the failure strain; while ductile failure is shown by a gradual decrease in the supported stress. A third common behavior is "strain hardening", shown by a gradual increase in the supported stress with axial strain.

Since the samples may have connected porosity (ie., internal porosity that is connected so that the pressure fluid could flow into the sample), we jacket them with a polyolefin (heat shrinkable) tubing secured to hardened steel or tungsten carbide endpieces to prevent contact with the pressure fluid. No lubricant is used at the endpiece-sample interface. The few runs in which the jacket leaked were evident immediately by the much lower strength of the sample.

We used three apparatus over the course of this work, depending on the strain rate. For the quasi-static strain rate of 10^{-4} s^{-1}, we used the biaxial stress apparatus shown in Fig. 3 for strain rates between 10^{-2} and 10^{2} s^{-1} we use the intermediate strain rate apparatus shown in Fig. 4; and for the 10^{3} s^{-1} work the Hopkinson split bar apparatus shown in Fig. 5. Each of these is described briefly below.

A complete description of the biaxial stress apparatus is given in Ref 13. The apparatus has two independent pressure manifolds to provide the confining pressure and to apply the axial load. All operations are done remotely using air-actuated valves. The length of the sample is measured using an LVDT external to the pressure cell, with corrections made for the compliances of the parts of the load chain included in the indicated displacement. We measure the pressure using a Teledyne-Taber gauge at pressures to 50 MPa and a manganin resistance gauge at higher pressures. The axial load is measured using a tungsten carbide load cell inside the pressure vessel, in contact with the sample. All voltage measurements are made with a HP3497A digital voltmeter, having a resolution of 10^{-6} volts, under control of an LSI 11/23 microcomputer; and the load-displacement data are plotted on an x-y recorder using the digital/analog output of the computer. The strengths at various strains are found from printed data tables, while the effective Young's modulus is obtained from the initial slope of the load-displacement curve on the x-y recorder

The intermediate strain rate apparatus (also known as BARF, the acronym of "Breaks All Rocks Fast") originally was developed to make high pressure-intermediate strain rate measurements on geologic materials. Strain rates of less than 10^{-2} s^{-1} at high confining pressures are fairly easy to obtain. Strain rates in the range 10^{-2} to 10^{5} s^{-1} can be obtained using various techniques, but only at ambient confining pressures. BARF uses a rotating cam (Fig. 4) to provide an axial load to a right circular cylinder sample inside a pressure vessel. The strain rates for a 2.54cm long sample can be varied from 10^{-2} to 10^{2} s^{-1} at confining pressures to 1000 MPa (145,000 Psi). To date the apparatus has been used to pressures of 200 MPa at 10^{-2} s^{-1}, to 30 MPa at 10^{-1} s^{-1}, and to 10 MPa at 10^{2} s^{-1}. Sample displacement is measured inside the pressure vessel using a linear potentiometer or a magnetic eddy current gauge. Axial load also is measured internally using a tool steel or a tungsten carbide load cell. We measure the confining pressure using an internal manganin gauge or an external Teledyne-Taber gauge. Since the experimental times in this work range from 1 second to 500 microseconds, the voltage data are acquired using a 100 kHz analog to digital card (ADAC Model 1023 AD) in an LSI 11/73 microcomputer. This 12 bit card has a resolution of 1 part in 4096. The fast times also mean that the confining pressure cannot be controlled manually, as in the quasi-static experiment, or with fast servo-systems. Instead, the pressure fluid is gas so that the decrease in volume of the vessel as the piston enters to provide axial displacement results in a negligible increase in pressure.

The Hopkinson split bar apparatus is described in Ref. 14 and shown in Fig. 5. The right circular cylinder sample is 0.6cm long and 1.27cm in. diameter and is glued between the input and output bars, made of aluminum. A heavy cylinder is accelerated down a tube using compressed air and creates the input stress pulse as it hits the input bar. The pulse is measured by the strain gauges on the input bar, passes through the sample, and the transmitted pulse measured by strain gauges on the output bar. Voltage outputs from the strain gauge bridges are amplified and displayed on oscilloscopes, where they are photographed. The photos are digitized and the strain gauge-time data analyzed to give the stress-strain-time history of the experiment. The

experiment is designed so that mechanical equilibrium can be assumed (there is time for several sound wave transits between sample and gauges) and results in strain rates of a few times 10^3 s^{-1}. Although some work has been done at confining pressures to 10 MPa and at various tempereatures[15], our two preliminary experiments were at ambient pressure and temperature.

RESULTS

Forty-two experiments were made at a strain rate of 10^{-4} s^{-1}, seventeen at 10^{-2} s^{-1}, ten at 10^{-1} s^{-1}, and four at rates greater than 10^3 s^{-1}. A typical shear stress-axial strain plot is shown in Fig 2. None of the experiments showed brittle failure, indicated by a sudden decrease in the load carried by the sample. The experiments at 0.1 MPa confining pressure showed a small decrease in the shear stress after a broad maximum, normally interpreted as simple plastic flow. All experiments at higher confining pressures showed an increasing shear stress with axial strain, which we call "work hardening". Since there is no clear "failure strength", we arbitrarily select the stresses at 3% and at 5% axial strain as a measure of the "strength" of the material. Another possibility is to attempt to define the point at which the shear stress-axial strain curve departs from a straight line at low stresses, and call that the failure strength. This was not done because of the guessing required to draw the line and because the material clearly could sustain larger loads at higher strains.

A summary of the data is given in Table 2 for the 10^{-4} s^{-1} strain rate, Table 3 for the 10^{-2} s^{-1} rate, in Table 4 for the 10^{-1} s^{-1} rate and in Table 5 for the rates greater than 10^3. Figure 6 is a plot of the 3% axial strain data from the present experiments. The jacket in experiment 016 leaked, and in 020 it was purposefully punctured to evaluate the effect of the high pressure gas coming into contact with the sample. The calculated stresses and strains are engineering values, using the ambient pressure dimensions of the samples.

Stresses are precise to about 3% and strains to about 1%.

DISCUSSION

Since these are the first failure curve data for a LOVA propellant and only the second set for any gun propellant at high pressures, there is not an "expected" behavior. The normal course for failure in most geologic materials, which often show properties similar to energetic materials[16], is for the failure strength to increase monotonically with confining pressure with a decreasing derivative. These data generally are represented in constitutive models by two straight line segments or by a quadratic. The results for a very fast burning gun propellant, shown in Figure 1, are typical. Not much is known about strain rate effects except that higher strain rates tend to result in higher failure strengths and in a change of failure mode from ductile to brittle. These qualitative features often are represented by some form of exponential term in the constitutive model for material strength.

The present data show a strong dependence of failure strength on confining pressure and on strain rate. The strength under quasi-static loading increases by a factor of 6 over the pressure range found in the interior ballistic cycle (0.1 - 400.0 MPa). Over the range 0.1 - 200.0 MPa of the 10^{-2} data, the strength increases by a factor of three; and over the smaller range of 30 MPa by 1.3. The pressure derivative of the failure strength is about the same for all strain rates.

The second remarkable feature is the "strain hardening" found in all experiments at pressures greater than 0.1 MPa. Each stress-strain path showed a region that could be called "elastic", generally up to axial strains of .01 or so. Beyond those strains, the material behaves plastically, supporting ever-increasing loads. This is significant in the hazards assessment of the material since it means that, at high confining pressures and at these strain rates, the material remains competent and does not fragment. Whether this is relevant depends on how well the stress-strain-time space of these experiments maps onto the history of the propellant grain during the ballistic cycle.

Finally, using these limited data, we can make some estimate of the strain rate dependence of the strength. Figure 7 is plot of the shear stress at 3% axial strain at 0.1 MPa confining pressure for the various strain rates. Had we not plotted the point at $2.6(10^3)$, we would leap to the conclusion that the strength depends exponentially on the strain rate. However, owing to the preliminary nature of all of these data, we simply present them and use them as a guide for the next experiments.

There are at least two other matters to consider in evaluating these data. First, all experiments were made at room temperature. In the ballistic cycle, the times are short enough so that it is a good estimate that the bulk temperature of the (initially) large grain does not change much from ambient. However, there is a large thermal gradient from the burning surface to the nominal bulk temperature that results in thermal stresses that must be added to the mechanical stresses of collision. Additionally, the complete hazards assessment of a propellant must include data over its service temperature range. We anticipate at least as large effects in the strength owing to a $100^{o}C$ change in temperature as those owing to pre sure and strain rate.

The second matter concerns the porosity of the grain itself. The amount of porosity and the degree to which it is connected, ie., the ease with which a high pressure fluid can flow through the porosity, are important in the ability of the bulk grain to support shear loads on its surface. In the two experiments in which this effect was evaluated, we found that the porosity at 30.0 MPa was connected enough to make the effective stress on the material (the applied stressless the pressure of the pressure fluid in the connected porosity) the same as the applied stress at lower confining pressures, and the sample 016 showed the same failure strength as those at lower confining pressures. (A good discussion of effective stress can be found in Ref. 17). At 100.0 MPa, the jacket of sample 020 was deliberately cut so that gas could flow into the porosity. The resulting small decrease in strength leads us to conclude that the initial prosity is low and poorly connected. For propellant grain designers low, poorly connected porosity means higher failure strengths.

CONCLUSION

These initial data show that the failure strength of this LOVA depends strongly on the confining pressure and strain rate. This means that the grain-grain stresses generated during loading of the packed bed during the early part of the ballistic cycle may be more important in analyzing grain failure than the stresses owing to grain-breech or grain-projectile collisions during the late part. Further, the increasing slope of the failure curve is an anomaly among all materials of which we are aware. It is not particularly important in this application owing to the limited pressures involved. However, it is relevant to the vulnerability of this material to high stress-high strain rate events, such as impacts by bullets or shrapnel. In these events, the stresses involved are several times those of the ballistic cycle, and the strain rates are higher than those of this work. The immediate suggestion is to exploit the reasons this failure curve has this anomalous shape to decrease even further its sensitivity to stress.

ACKNOWLEDGEMENT

We wish to thank Mr. Nick Brazell and Mr. Don Breithaupt for performing and analyzing the Hopkinson split bar experiments. This work was supported, in part, by BRL Project Orders 04-84 and 19-85.

This work was performed under the auspices of the U.S. Department of Energy by Lawrence Livermore National Laboratory under contract No. W-7405-Eng-48.

REFERENCES

1. See, e.g., P.B. Butler, M.F. Lembeck, and H. Krier, "Modeling of Shock Development and Transition to Detonation Initiated by Burning Porous Propellant Beds", Combustion and Flame 46, 75-93 (1982).

2. Douglas E. Kooker and Ronald D. Anderson, "Closed-Bomb Combustion Simulation of Hivelite Solid Propellant", 3d JANNAF Propulsion Systems Hazards Meeting, Los Alamos, NM, 13-15 July 1983.

3. M.M. Carroll and A.C. Holt, "Static and Dynamic Pore-Collapse Relations for Ductile Porous Materials", J. Appl. Phys. 43, 1627-1636 (1972).

4. O.R. Walton, J. Bryan, C. Snell, J.M. Thompsen, and M. Goodrich, "Effects of Porosity, Strength, and Water Content on Attenuation of Stress Generated by Subsurface Explosions in Soils", Lawrence Livermore National Laboratory UCRL-79113, 1977.

5. K.K. Kuo, V. Yang, and B.B. Moore, "Intergranular Stress, Particle Wall Friction, and Speed of Sound in Granular Propellant Beds", J. of Ballistics 4, 697-730 (1980).

6. M. Costantino, "Volumes and Sound Speeds of Two Gun Propellants at High Pressure", Propellants, Explosives, Pyrotechnics 9, 22-29 (1984).

7. S. Nicolaides, D.A. Wiegand, and J. Pinto, "The Mechanical Behavior of Gun Propellant Grains and its Role in Interior Ballistics", 16th JANNAF Structures and Mechanical Behavior Subcommittee Meeting, Colorado Springs, CO, 11-13 Dec 1979. CPIA Pub 311, 1980 pp 145-165, and references therein.

8. A.M. Weston and E.L. Lee, "Response of Porous Beds to Rapid Gas Pressurization", Lawrence Livermore National Laboratory UCID-19697.

9. A.E. Abey and K. Keller, Lawrence Livermore National Laboratory, unpublished data.

10. S. Nicolaides, D.A. Wiegand, and J. Pinto, "The Mechanical Behavior of Gun Propellants in Interior Ballistics", U.S. Army Armamn the Mechanical Properties of Gun Propellants", JANNAF Propulsion Meeting, Monterey, CA, Oct 1980. CPIA Pub 330 Vol. 1, p289.

13. Marc Costantino and Donald Ornellas, "The Experimental High Pressure Equation of State of a Very Fast Burning Gun Propellant", JANNAF Combustion Meeting, Laurel, MD, 1-5 Oct 1984. (Also available as Lawrence Livermore National Laboratory UCRL 91565).

14. K.G. Hoge, Appl. Polymer Symposia 5, 19-40 (1967)

15. D. Breithaupt, Private communication.

16. M. Costantino, "The Relevance of Rock Mechanics to Gun Propellants", Third International Gun Propellant Symposium, Dover, NJ. 30 Oct. - 1 Nov. 1984.

17. J.C. Jaeger and N.G.W. Cook, Fundamentals of Rock Mechanics, Chapman and Hall, 1969.

TABLE 1. Composition of the LOVA propellant used in this work.

COMPONENT	WEIGHT %
RDX	76.0
CAB (Cellulose Acetate Butyrate)	12.0
ATC (Acetyl Triethylcitrate)	7.6
NC (Nitrocellulose, 12.6%N)	4.0
Ethyl Centralite	0.4
	100.0

TABLE 2. Maximum Shear stress at 3% and at 5% axial strain at a strain rate of 10^{-4} s^{-1}.

SAMPLE	CONFINING PRESSURE (MPa)	SHEAR STRESS at 3% STRAIN (MPa)	SHEAR STRESS at 5% STRAIN (MPa)
L01	0.1	8.5	10.9
L02	0.1	8.3	10.1
L03	0.1	8.7	11.1
L04	0.1	8.8	11.3
L05	0.1	8.8	11.5
L06	0.1	8.9	11.6
L07	0.1	8.6	11.1
L09	3.0	9.4	12.3
L10	3.0	9.4	12.3
L11	3.0	9.5	12.4
L12	10.0	10.0	12.9
L13	10.0	10.0	12.9
L14	10.0	9.8	12.9
L15	30.0	11.3	14.4
L16	30.0	11.1	14.2
L17	30.0	11.2	14.3
L19	100.0	16.2	19.2
L20	100.0	16.0	19.1
L21	100.0	15.9	18.7
L23	225.0	27.0	19.5
L24	225.0	28.9	32.0
L25	225.0	28.8	31.5
L38	300.0	36.7	40.4
L39	300.0	36.9	40.6
L41	400.0	53.6	58.6
L42	400.0	53.8	58.9

TABLE 3. Maximum shear stress at 3% and at 5% axial strain at a strain rate of 1.09 (10^{-2}) s^{-1}.

SAMPLE	CONFINING PRESSURE (MPa)	SHEAR STRESS at 3% STRAIN (MPa)	SHEAR STRESS at 5% STRAIN (MPa)
005	0.1	13.0	14.1
006	0.1	13.2	13.3
007	0.1	13.2	14.4
008	3.0	13.3	15.3
009	3.0	13.1	15.3
010	3.0	13.5	15.4
011	10.0	13.8	16.4
012	10.0	13.5	16.3
013	10.0	13.5	16.1
014	30.0	15.0	17.8
015	30.0	16.7	18.5
016	30.0	13.3	16.4
017	100.0	22.4	25.0
018	100.0	23.2	25.6
019	100.0	23.2	25.6
020	100.0	20.2	23.0
022	200.0	38.0	-----

TABLE 4. Maximum shear stress at 3% and at 5% axial strain at a strain rate of 0.73 (10^{-1}) s^{-1}.

SAMPLE	CONFINING PRESSURE (MPa)	SHEAR STRESS at 3% STRAIN (MPa)	SHEAR STRESS at 5% STRAIN (MPa)
023	0.1	14.3	13.6
025	0.1	12.0	11.5
026	0.1	14.9	14.6
027	3.0	15.4	16.4
028	3.0	15.1	16.4
029	10.0	15.4	17.5
030	10.0	15.6	18.0
031	30.0	18.8	21.7
032	30.0	16.8	19.2

TABLE 5. Maximum shear stress at 3% and at 5% axial strain at strain rates greater than 10^3 s^{-1}. Confining pressure is 0.1 MPa.

SAMPLE	STRAIN RATE (s^{-1})	SHEAR STRESS at 3% STRAIN (MPa)	SHEAR STRESS at 5% STRAIN (MPa)
H001	$2.6(10^3)$	38.8	45.7
H002	$2.6(10^3)$	40.3	46.4
H003	$1.7(10^3)$	29.8	33.7
H004	$1.5(10^3)$	29.8	33.7

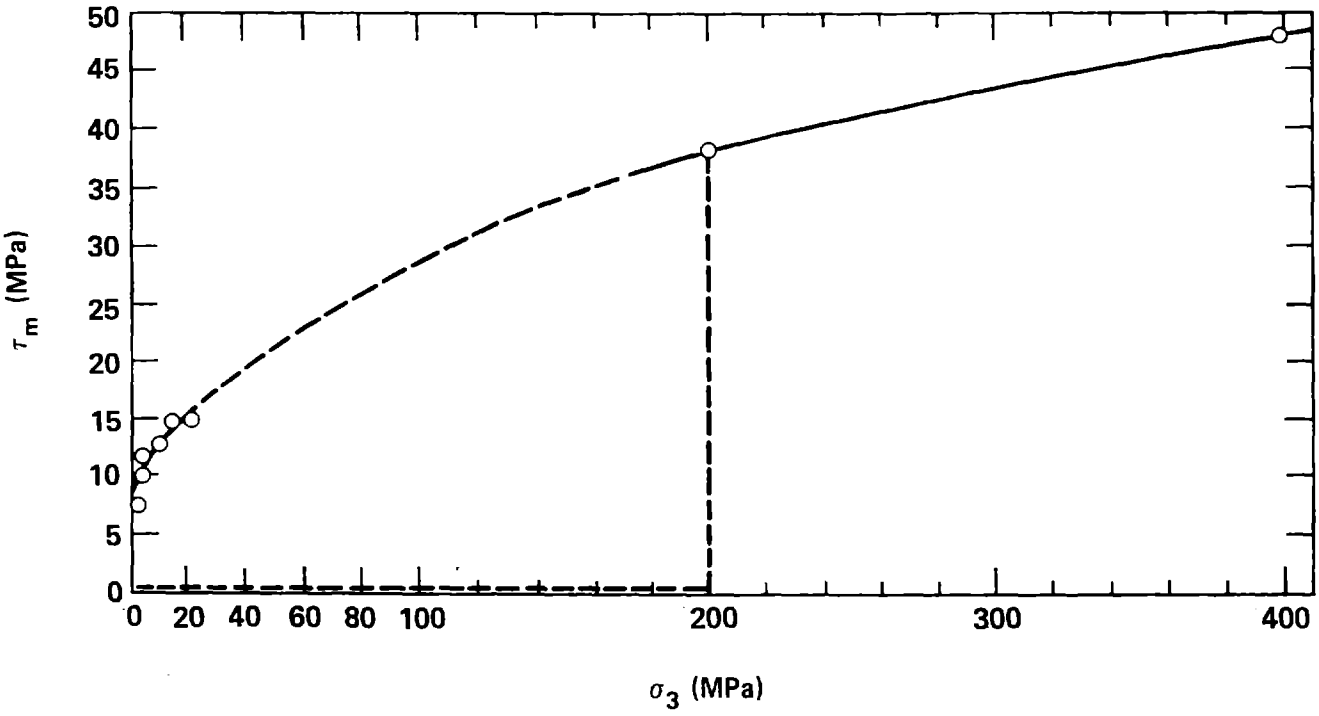

Figure 1. Failure curve for a very fast burning propellant. The dashed line is the loading path. (From Ref. 13).

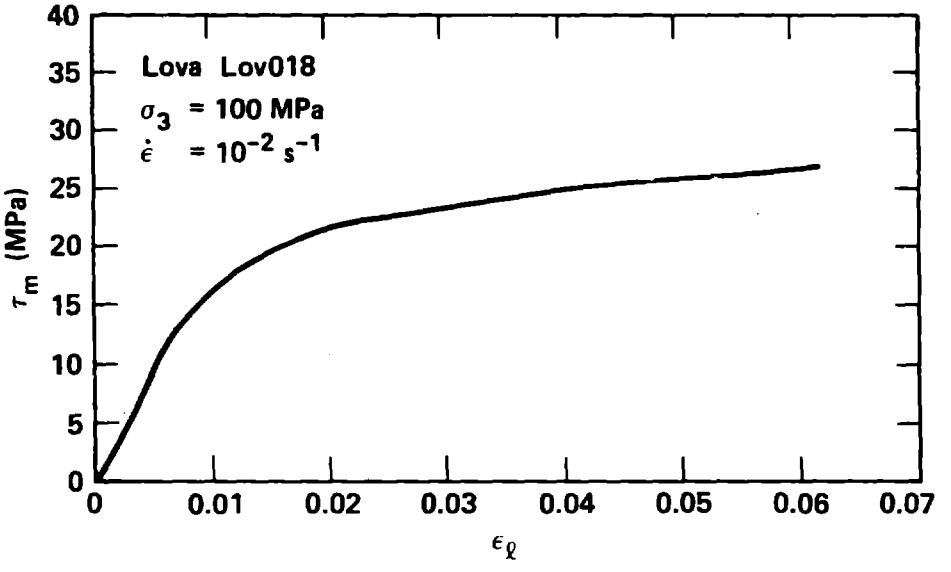

Figure 2. The shear stress-axial strain path for a LOVA propellant. The confining pressure is 100 MPA and the strain rate is 10^{-2} s^{-1}.

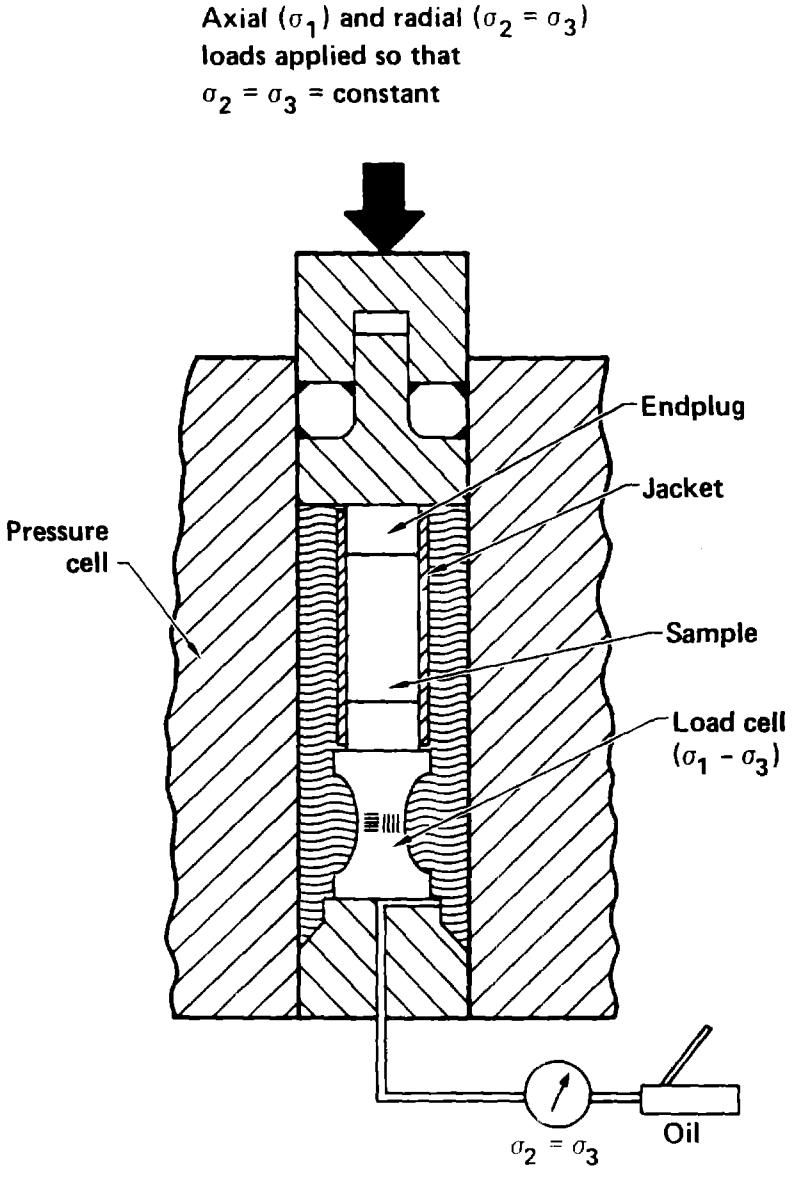

Figure 3. Schematic of the apparatus used to obtain failure strength data at 10^{-4} s^{-1} strain rate.

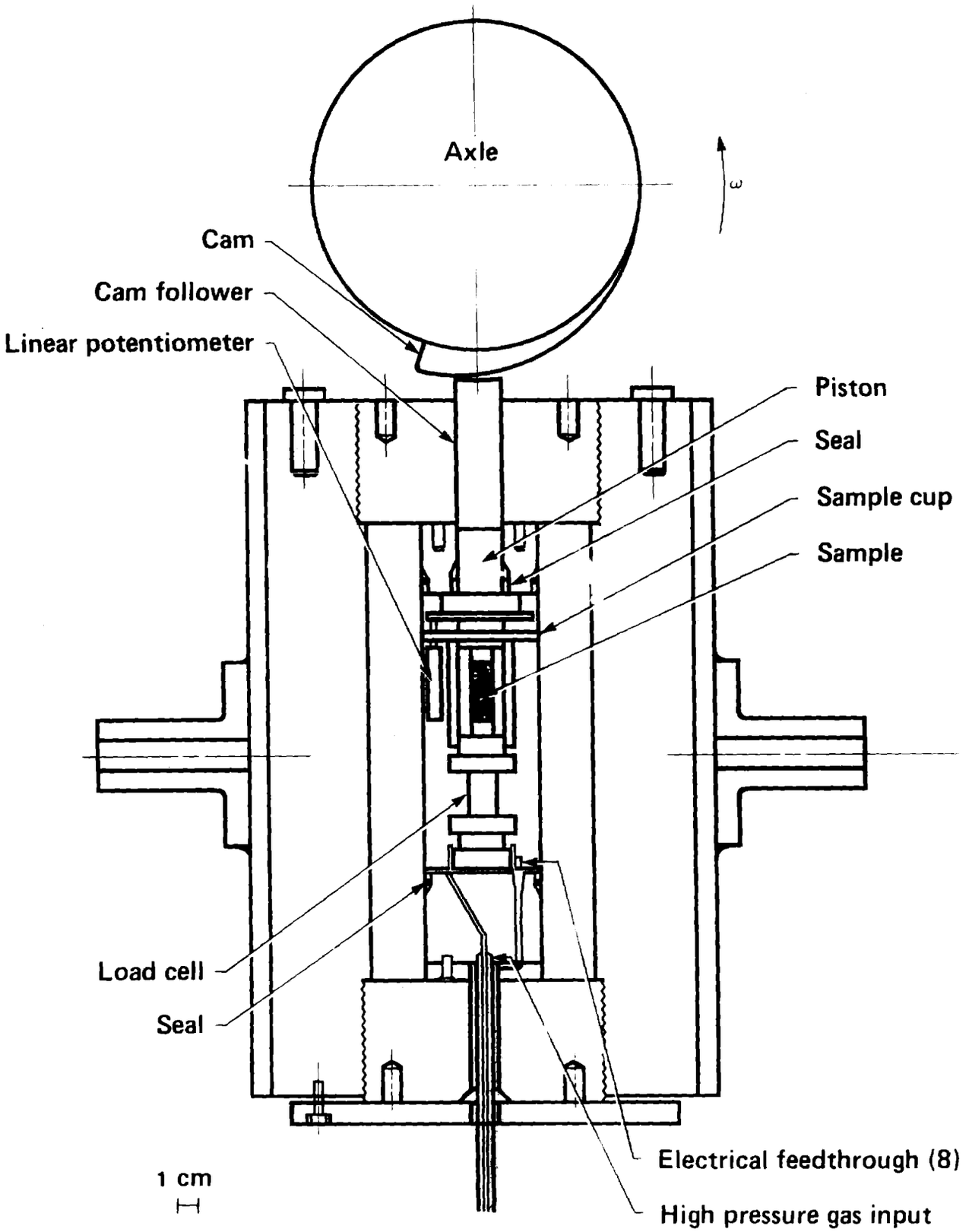

Figure 4. Schematic of the intermediate strain rate apparatus used to obtain failure strength data at strain rates of 10^{-2} s^{-1} and 10^{-1} and s^{-1}.

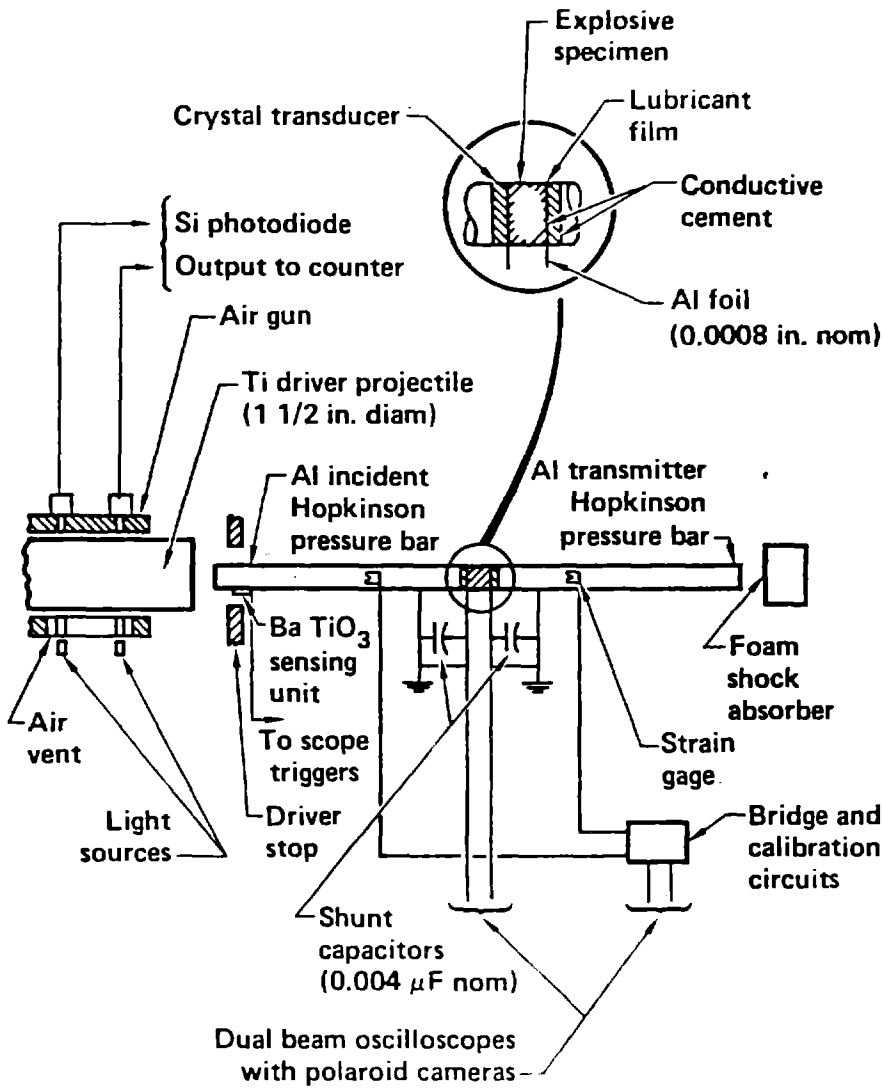

Figure 5. Schematic of the Hopkinson split bar apparatus used to obtain failure strength data a strain rates greater than 10^3 s^{-1}.

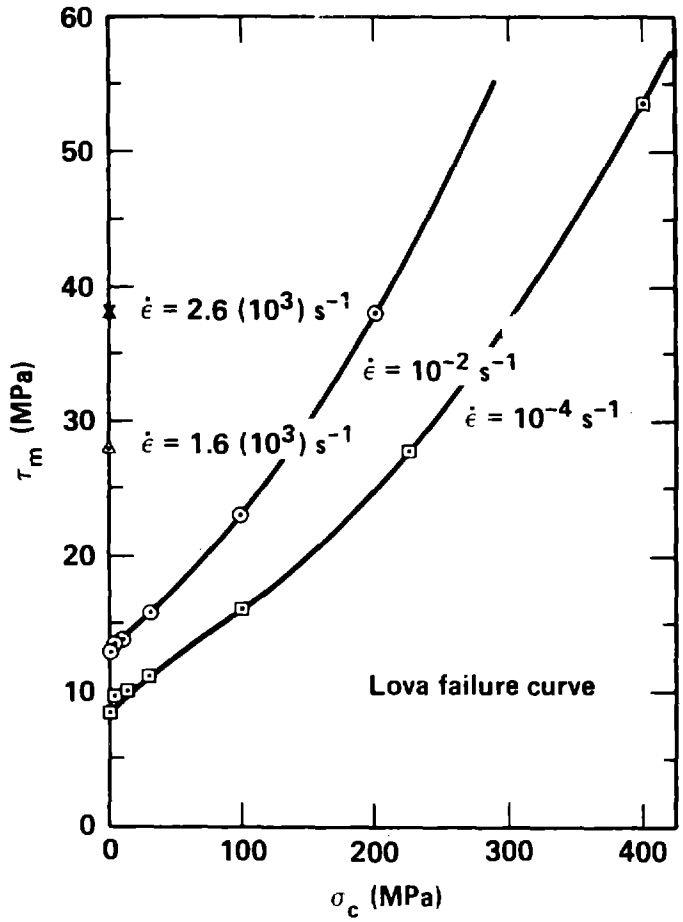

Figure 6. Maximum shear stress vs confining pressure at 3% axial strain at various strain rates for a LOVA propellant.

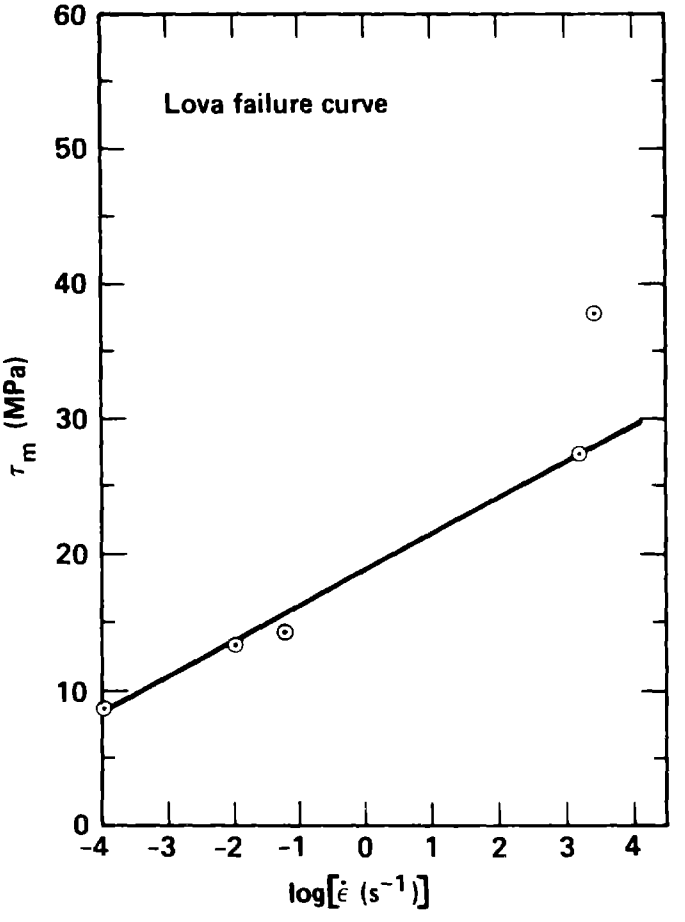

Figure 7. Maximum shear stress at 3% axial strain vs long (strain rate) at a confining pressure of 0.1 MPa.